

# Loss of ASAP1 in the MMTV-PyMT model of luminal breast cancer activates AKT, accelerates tumorigenesis, and promotes metastasis

Caroline Schreiber<sup>a</sup>, Annette Gruber<sup>a</sup>, Sven Roßwag<sup>a</sup>, Supriya Saraswati<sup>a</sup>, Shannon Harkins<sup>a</sup>, Wilko Thiele<sup>a,b</sup>, Zahra Hajian Foroushani<sup>c</sup>, Natalie Munding<sup>c</sup>, Anja Schmaus<sup>a,b</sup>, Melanie Rothley<sup>a,b</sup>, Arno Dimmler<sup>d</sup>, Motomu Tanaka<sup>c,e</sup>, Boyan K. Garvalov<sup>a,\*\*,1</sup>, Jonathan P. Sleeman<sup>a,b,\*,1</sup>

<sup>a</sup> European Center for Angioscience (ECAS), Medical Faculty Mannheim, Heidelberg University, 68167, Mannheim, Germany

<sup>b</sup> Institute for Biological and Chemical Systems - Biological Information Processing (IBCS-BIP), Karlsruhe Institute of Technology (KIT) Campus North, D-76344 Karlsruhe, Germany

<sup>c</sup> Physical Chemistry of Biosystems, Institute of Physical Chemistry, Heidelberg University, 69120, Heidelberg, Germany

<sup>d</sup> Vincentius-Diakonissen-Kliniken, 76135, Karlsruhe, Germany

<sup>e</sup> Center for Integrative Medicine and Physics, Institute for Advanced Study, Kyoto University, 606-8501, Kyoto, Japan

## ARTICLE INFO

### Keywords:

ASAP1  
Luminal breast cancer  
Metastasis  
Invasion  
AKT  
Hyperplasia  
MMTV-PyMT

## ABSTRACT

ASAP1 is a multi-domain adaptor protein that regulates cytoskeletal dynamics, receptor recycling and intracellular vesicle trafficking. Its expression is associated with poor prognosis in a variety of cancers, and can promote cell migration, invasion and metastasis. Although amplification and expression of ASAP1 has been associated with poor survival in breast cancer, we found that in the autochthonous MMTV-PyMT model of luminal breast cancer, ablation of ASAP1 resulted in an earlier onset of tumor initiation and increased metastasis. This was due to tumor cell-intrinsic effects of ASAP1 deletion, as ASAP1 deficiency in tumor, but not in stromal cells was sufficient to replicate the enhanced tumorigenicity and metastasis observed in the ASAP1-null MMTV-PyMT mice. Loss of ASAP1 in MMTV-PyMT mice had no effect on proliferation, apoptosis, angiogenesis or immune cell infiltration, but enhanced mammary gland hyperplasia and tumor cell invasion, indicating that ASAP1 can accelerate tumor initiation and promote dissemination. Mechanistically, these effects were associated with a potent activation of AKT. Importantly, lower ASAP1 levels correlated with poor prognosis and enhanced AKT activation in human ER+/luminal breast tumors, validating our findings in the MMTV-PyMT mouse model for this subtype of breast cancer. Taken together, our findings reveal that ASAP1 can have distinct functions in different tumor types and demonstrate a tumor suppressive activity for ASAP1 in luminal breast cancer.

## 1. Introduction

Breast cancer is the most prevalent type of cancer in women in the Western world. Advances in early diagnosis and the development of therapeutic strategies have improved the life expectancy of patients considerably, with the relative 10-year survival of breast cancer patients in Germany currently at 82% [1]. However, around 25% of these women eventually succumb to their disease, mainly due to the consequences of metastasis.

Breast cancers can be stratified into different molecular subtypes

based on the expression of the estrogen receptor (ER), progesterone receptor (PR) and human epidermal growth factor receptor 2 (HER2) [2, 3]. Each subtype has a different prognosis and requires a different treatment regimen [4]. Luminal breast cancer, the most frequent type of breast cancer, is positive for the expression of ER and PR, but is mainly negative for HER2. Luminal breast cancers are subdivided into luminal A and luminal B according to their proliferation rate. Basal tumors, on the other hand, are negative for ER, PR and HER2 (triple negative) and have the worst prognosis of all breast cancer subtypes.

ASAP1 (ArfGAP with SH3 domain, ankyrin repeats and PH domain 1) is a cytoplasmic adaptor protein that is also known as AMAP1 and

\* Corresponding author. European Center for Angioscience (ECAS), Medical Faculty Mannheim, Heidelberg University, 68167 Mannheim, Germany.

\*\* Corresponding author.

E-mail addresses: [boyan.garvalov@medma.uni-heidelberg.de](mailto:boyan.garvalov@medma.uni-heidelberg.de) (B.K. Garvalov), [jonathan.sleeman@medma.uni-heidelberg.de](mailto:jonathan.sleeman@medma.uni-heidelberg.de) (J.P. Sleeman).

<sup>1</sup> These authors contributed equally to this work.

## Abbreviations

$\alpha$ SMA	alpha smooth muscle actin
ANOVA	analysis of variance
ASAP1	ArfGAP with SH3 domain, ankyrin repeats and PH domain 1
BSA	bovine serum albumin
CAF	cancer-associated fibroblast
CD2AP	CD2-associated protein
CK14	cytokeratin-14
DMEM	Dulbecco's modified Eagle's medium
DMSO	dimethyl sulfoxide
ER	estrogen receptor
ERK	extracellular signal-regulated kinase
FAK	focal adhesion kinase
FAP	Fibroblast activation protein
FCS	fetal calf serum
GAP	GTPase-activating protein
HER2	human epidermal growth factor receptor 2
IKK $\beta$	inhibitor of nuclear factor kappa-B kinase subunit beta

KO	knockout
LTR	long terminal repeat
MaSC	mammary stem cells
MEF	mouse embryonic fibroblast
m.f.p.	mammary fat pad
MMTV	mouse mammary tumor virus promoter
PDGFR $\alpha$	platelet-derived growth factor receptor alpha
PECAM-1	Platelet endothelial cell adhesion molecule 1
PI3K	phosphatidylinositol 3-kinase
PIPP	Phosphatidylinositol 4,5-bisphosphate 5-phosphatase
PR	progesterone receptor
PyMT	polyoma middle tumor-antigen
SEM	standard error of the mean
SFK	Src family kinases
SH3	SRC Homology 3
TCGA	The Cancer Genome Atlas
TUNEL	Terminal deoxynucleotidyl transferase dUTP nick end labeling
WT	wild-type

DDEF1. It contains multiple domains, including a BAR domain that mediates sensing or induction of membrane curvature, an ArfGAP domain with phospholipid-dependent GAP activity mainly for Arf1 and Arf5, and proline-rich and SH3 domains that allow the ASAP1 protein to interact with a variety of intracellular regulatory proteins including c-Src, FAK, paxillin, cortactin, CrKL, CD2AP and IKK $\beta$  [5–10]. The ASAP1 protein localizes to the perinuclear region, membrane ruffles and focal adhesions [11]. Functionally, ASAP1 coordinates cytoskeletal dynamics [7,9], receptor recycling [12], vesicle formation [13] and cell motility [12,14–16].

ASAP1 is amplified in various tumor entities, and its expression often correlates with poor survival [17–21]. Previously, we have shown that ASAP1 promotes the migration and metastasis of pancreatic tumor cells *in vivo* and correlates with poor metastasis-free and overall survival of colorectal cancer patients [15]. ASAP1 has also been reported to be amplified in some breast cancers, and high ASAP1 expression is associated with reduced metastasis-free survival of triple-negative breast cancer patients [8,22,23].

To investigate the role of ASAP1 in tumor progression and metastasis *in vivo* and to analyze its potential use as a therapeutic target, we examined the consequences of ASAP1 deletion in the MMTV-PyMT mouse model of luminal breast cancer. MMTV-PyMT mice express the polyoma middle T oncogene (PyMT) under the control of the MMTV LTR promoter [24–26]. By the age of 9 weeks the mice establish solid mammary adenocarcinomas that correspond to the luminal subtype of human breast cancer and metastasize to the lung [27,28]. In order to obtain PyMT ASAP1 KO mice, we crossed MMTV-PyMT mice with ASAP1 loss-of-function (*Asap1*<sup>GT/GT</sup>) mice.

Analysis of the PyMT ASAP1 KO mice revealed that, contrary to expectation, deletion of ASAP1 in tumor cells promoted tumor formation and metastasis. ASAP1-deficient PyMT tumor cells exhibited an increased activation of AKT signaling. Consistently, low ASAP1 expression correlated with high levels of activated AKT and with poor survival in human luminal breast cancers. Together, our results indicate that ASAP1 plays a context-dependent role in breast cancer, and can either suppress tumor formation or promote metastasis depending on the breast cancer subtype.

## 2. Materials and methods

### 2.1. Mouse mammary tumor model

The FVB;*Asap1*<sup>GT</sup> mice which we have previously established [25] were crossed into the FVB; MMTV-PyMT mouse model. Specifically, *PyMT;Asap1*<sup>+GT</sup> male mice were crossed with *Asap1*<sup>+GT</sup> females to obtain *PyMT;Asap1*<sup>+/+</sup> (PyMT WT) and *PyMT;Asap1*<sup>GT/GT</sup> (PyMT ASAP1 KO) female mice. The mice were monitored twice a week for tumor growth, and tumor size was recorded after first palpation. Tumor volume was calculated by using the formula  $4/3\pi(r_{\text{length}} \cdot r_{\text{width}} \cdot r_{\text{depth}})$ . Tumor burden represents the sum of tumor volumes of all tumors per mice. All mice were sacrificed by cervical dislocation at the age of 13 weeks ( $91 \pm 3$  days), and tumors and lungs were removed for analysis. Numbers of metastases were counted macroscopically using a stereomicroscope. The metastatic index represents the number of lung metastases per cm<sup>3</sup> of total tumor burden. All mice were maintained under housing conditions in accordance with German government and institutional guidelines and regulations. Permission for the experiments in this study was granted by the local authorities (Permit number 35–9185.81/G-298/16). Genotyping was performed as previously described [24,25].

### 2.2. Cell culture

PyMT tumor cell lines were isolated from tumors taken from PyMT WT and PyMT ASAP1 KO mice. Tumors were mechanically dissociated using a scalpel, then incubated in 0.05% trypsin for 4 min at 37 °C. Normal growth medium (see below) was added, the cell suspension was passed through a 40  $\mu$ m cell strainer, washed in medium and transferred to a cell culture dish. Cell lines were grown for  $\geq 14$  passages before *in vivo* and *in vitro* experiments were carried out. MEFs were isolated and cultured as previously described [25]. All cells were passaged in DMEM (Life Technologies) supplemented with 10% fetal calf serum (FCS, Sigma), 1% penicillin/streptomycin (Life Technologies) and 2 mM L-glutamine (Life Technologies).

### 2.3. Mammary fat pad injection

Orthotopic injection of  $10^6$  tumor cells, and where indicated, equal numbers of MEFs was used to generate tumors in mammary fat pad #4 of 8–10 weeks old FVB WT or FVB ASAP1 KO female mice. Mice were

palpated twice a week to monitor tumor growth. When tumors reached a diameter size of 2 cm, mice were euthanized and tumors and lungs were removed for analysis. To assess lung metastasis, mRNA was isolated from 3 separate lobes per lung, PyMT expression was assessed by qPCR and normalized to WT lungs set to 1. Permission for these experiments in this study was granted by the local authorities (Permit number 35-9185.81/G-40/18).

#### 2.4. Histological analysis

Tumors were excised, fixed in formalin, dehydrated and embedded in paraffin. Sections with a thickness of 5  $\mu\text{m}$  were re-hydrated, and antigen retrieval was performed using citrate buffer (DAKO, Santa Clara, CA, USA). The following antibodies were used: ASAP1 (#NBP2-48909, 1:300, Novus Biologicals), Ki67 (#ab15580, 1:500, abcam), CD31/PECAM-1 (sc-1506, 1:400 Santa Cruz), F4/80 (#ab6640, 1:200, abcam), CK14 (PRB115P, 1:500, Covance). Staining was detected using an ABC Kit and visualized with Nova Red (Vector Labs). For immunofluorescence staining, a secondary antibody conjugated with Alexa 488 (Invitrogen) was used, followed by counterstaining with diaminodiphenylindole (DAPI). Images were taken using an Axio Imager microscope (Zeiss). Images were quantified using ImageJ [29]. Microvascular density (MVD) was defined as the fraction of PECAM-1-positive area per image.

#### 2.5. Mammary whole mount staining

Mammary glands #4 were excised *post mortem*, mounted on a glass slide and fixed in 100% EtOH, chloroform and glacial acetic acid (ratio 6:3:1) for 2 h. Glands were stained in carmine alum and cleared in Rotihistol as previously described [30]. Whole mount images were captured on a Leica stereomicroscope and analyzed using ImageJ. Branching density was assessed using Sholl analysis, as previously described [30], which evaluates the number of intersections per mammary epithelia area ( $\text{N}/\text{mm}^2$ ). Ductal invasion represents the average length of the three longest ducts per gland.

#### 2.6. Immunofluorescence staining

Cells were seeded on glass substrates coated with the stacks of gelatin nanofibers and cultured for 4 days before the fixation. The nanofibers were deposited by electrospinning using a self-built electrospinner [31]. In brief, an 11 wt% solution of gelatin type A (Sigma-Aldrich) dissolved in a mixture of acetic acid, ethyl acetate, and distilled water (acetic acid: ethyl acetate, 3:2 by volume) was electrospun for 180 s at 23  $^{\circ}\text{C}$  [32]. The nanofibers were dried and chemically cross-linked by immersion into 0.2 M *N*-ethyl-*N'*-(dimethylaminopropyl) carbodiimide (EDC, Sigma-Aldrich) and 0.2 M *N*-hydroxysuccinimide (NHS, Sigma-Aldrich) in ethanol (4 h). The chemically cross-linked gelatin nanofibers were rinsed with 70% ethanol three times and dried in vacuum.

The cells were fixed in 4% paraformaldehyde in PBS for 15 min at room temperature, washed thrice with PBS and permeabilized with PBS containing 0.2% (w/v) Triton X-100 (Carl Roth) for 5 min. The samples were blocked with 3% (w/v) bovine serum albumin (BSA, Sigma-Aldrich) in PBS for 30 min at room temperature. For the immunohistochemical staining, the following affinity probes and antibodies were used: vinculin monoclonal antibody (7F9), Alexa Fluor 488 (# 53-9777-82, Thermo Fisher, 1:200) and Texas Red-X Phalloidin (T7471, Thermo Fisher, 1:500). Nuclei were stained with DAPI (Sigma-Aldrich, 1:1000). All the incubations were performed in PBS containing 3% (w/v) BSA for 1 h at room temperature, and rinsing was done with PBS.

Images were acquired with a Nikon C2 Plus confocal microscope (Nikon, Düsseldorf, Germany) equipped with a 60  $\times$  oil immersion objective. Cell morphology was analyzed using Fiji software. The area of each cell projected on the surface was calculated using the cell contour extracted from the confocal image. The cell shape was fitted to an ellipse

and the ratio of major and minor axis yielded the cellular aspect ratio. Focal adhesions (FAs), obtained from the maximal projection of confocal z-stacks, were binarized using the default thresholding. Continuous areas with sizes of 0.5–20  $\mu\text{m}^2$  were classified as FAs, and their number and size were measured for each cell.

#### 2.7. Proliferation assay

Cells were incubated for 72 h in 96-well plates, and DNA content (as a measure of cell proliferation) was analyzed using the CyQUANT proliferation assay (C35006, Thermo Fisher Scientific). Growth medium was removed, then 50  $\mu\text{L}$  of CyQUANT dye diluted 1:500 in 1x HBSS was added per well. Plates were incubated for 15 min at 37  $^{\circ}\text{C}$  to allow the CyQUANT dye to incorporate into DNA. Fluorescence was measured by excitation at 485 nm and detection of emission at 530 nm, at 25 positions in each well, using a Tecan Infinite M200 reader.

#### 2.8. Adhesion assay

24-well plates were coated with 20  $\mu\text{g}/\text{ml}$  fibronectin, 20  $\mu\text{g}/\text{ml}$  collagen I or 1% BSA overnight at 4  $^{\circ}\text{C}$ . Unspecific binding was prevented by blocking with 1% BSA for 30 min at 37  $^{\circ}\text{C}$ . PyMT WT or PyMT ASAP1 KO tumor cells were plated at a density of 200,000 cells per well, incubated on ice for 30 min and then allowed to adhere for 1 h at 37  $^{\circ}\text{C}$ . Cells were fixed with 70% EtOH and stained with 0.5% crystal violet. After crystal violet extraction with 10% HCl, absorbance at 595 nm was measured.

#### 2.9. Transwell invasion assay

50  $\mu\text{l}$  Matrigel HC (#354262, Corning) at a concentration of 0.6 mg/ml was added to transwell inserts (#3422, Corning) and incubated for 4 h at 37  $^{\circ}\text{C}$ . Subsequently 50,000 cells in DMEM/1% FCS were added on top of the Matrigel, and DMEM/10% FCS was added to the bottom compartment as a chemoattractant. For inhibitor experiments, 1  $\mu\text{M}$  AKT1/2 inhibitor (#A6730, Sigma) or DMSO in the same dilution was added to the upper and lower compartment. After 72 h, cells were fixed and stained with DAPI. Relative invasion was calculated as the ratio of the DAPI signal of the cells that had invaded onto the bottom surface of the insert (imaged following removal of the cells from the top surface) and the DAPI signal of the total cells (imaged before removal of the cells from the top surface).

#### 2.10. Retroviral transduction

Plat-E retroviral packaging cells [33] were transfected with 9  $\mu\text{g}$  empty pQCXIP vector, or with pQCXIP-ASAP1c [15] using FuGENE (Promega). Supernatants containing retroviruses were transferred to PyMT WT and ASAP1 KO cell lines. Transduced cells were selected with 2  $\mu\text{g}/\text{ml}$  puromycin.

#### 2.11. RNA isolation and qPCR

RNA was isolated using Trizol (Invitrogen) according to the manufacturer's protocol. Subsequently, 1.5–2  $\mu\text{g}$  of RNA was digested with 5 U DNase I (Thermo Fisher Scientific) for 30 min at 37  $^{\circ}\text{C}$ . The reaction was stopped by addition of EDTA and heat inactivation, then the RNA was transcribed into cDNA using Revert Aid H Minus reverse transcriptase (Thermo Fisher Scientific) according to the manufacturer's protocol. Gene expression was analyzed using a SYBR-Green mix (Promega) to perform real-time qPCR using the Step One Plus Realtime PCR System (Applied Biosciences) under the following PCR conditions: 15 sec 95 $^{\circ}\text{C}$ , 1 min 60 $^{\circ}\text{C}$ , 1 min 72 $^{\circ}\text{C}$ . The ribosomal protein P0 (RPLP0) was used as a housekeeping gene to normalize the data. The sequences of primer pairs used to amplify the indicated cDNAs were: mouse RPLP0 (for 5'- GGACCCGAGAAGACCTCCTT-3', rev 5'-

GCACATCACTCAGAATTTCAATGG); PyMT (for 5'-AACCCGA-GATGTCTAACCC-3', rev 5'CTCTCTCAGTTCCTCGTC-3'); mouse  $\alpha$ SMA (for 5' GTTCAGTGGTGCCTCTGTCA-3', rev 5'-ACTGGGACGA-CATGGAAAAG-3'); mouse tenascin (for 5'-CCTGTCCAATGACTG-CAGC-3', rev 5'-GGTACTCAGTGACCCGCATC-3').

## 2.12. Western blot analysis

Mouse tissues and cells for protein lysates were lysed in RIPA buffer, homogenized using a TissueLyser II (Qiagen, Venlo, Netherlands) and quantified using the BCA Protein Assay Kit (Thermo Fisher Scientific). PyMT WT and PyMT ASAP1 KO tumor cells were cultivated on uncoated 10 cm tissue culture dishes for 24 h before lysis. Lysates were subjected to 10% SDS-PAGE and transferred to a PVDF membrane. Protein expression was analyzed using rabbit anti-ASAP1 (7B12) [15], rabbit anti-FAK (06-543, 1:1000, Merck Millipore), rabbit anti-phospho FAK Y397 (44-624G, 1:1000, Thermo Fisher), rabbit anti-Src (ab47405, 1:1000, abcam), rabbit anti-phospho Src Y416 (#6943, 1:1000, Cell Signaling), rabbit anti-phospho AKT T308 (#9275, 1:1000, Cell Signaling), rabbit anti-AKT (sc-8312, 1, 1:200, Santa Cruz), rabbit anti-ERK (sc-93, 1:200, Santa Cruz), mouse anti-phospho ERK (#9106, 1:1000, Cell Signaling). Probing the membranes with mouse anti-vinculin antibodies (V4139, 1:50,000, Sigma) served as a loading control.

## 2.13. Bioinformatic analysis of TCGA data

Data for the bioinformatic analysis of human TCGA breast cancer cohort Pan Cancer Atlas [34] was retrieved from the cBioPortal (<https://www.cbioportal.org/>) [35,36]. AKT1/2/3\_PT308 protein expression was analyzed in luminal tumor samples with or without an ASAP1 gain or amplification. ASAP1 mRNA and protein expression data in ER-positive and ER-negative breast tumors were analyzed in the TCGA

breast cancer cohort Firehouse Legacy. Kaplan-Meier survival analysis was performed with data from human ER-positive breast cancers obtained from the analysis platform KM Plotter (<https://kmplot.com/analysis/>) [37] using „Auto select best cutoff“.

## 2.14. Statistical analysis

All statistical analyses were performed in GraphPad Prism. Differences between two groups were analyzed using a two-tailed unpaired Student's t-test. Differences between more than two groups were analyzed by a one-way ANOVA test together with Dunnett's multiple comparisons test. For comparison of tumor growth curves at different time points, two-way ANOVA with Šidák's multiple comparisons test was used. Comparison of survival curves was performed using the log-rank (Mantel-Cox) test. P values < 0.05 were considered statistically significant and indicated as follow: \* $P < 0.05$ , \*\* $P < 0.01$ , \*\*\* $P < 0.001$ .

## 3. Results

### 3.1. Loss of ASAP1 accelerates tumor development and promotes lung metastasis

To determine how loss of ASAP1 affects tumor progression and metastasis, we crossed the ASAP1 gene trap mouse line into the well-characterized mouse mammary tumor model MMTV-PyMT [24,25]. The resulting female MMTV-PyMT; *Asap1*<sup>+/+</sup> (PyMT WT) and MMTV-PyMT; *Asap1*<sup>GT/GT</sup> (PyMT ASAP1 KO) mice (Fig. 1a) were assessed weekly for tumor development. Mice deficient for ASAP1 showed a trend towards an earlier tumor onset (Fig. 1b) and tumor growth was enhanced when compared to PyMT WT mice (Fig. 1c). When mice had to be sacrificed at week 13 due to increased tumor burden in the PyMT ASAP1 KO mice, we could detect increased surface metastasis in the lungs of PyMT ASAP1 KO mice (Fig. 1d and e). These data suggest

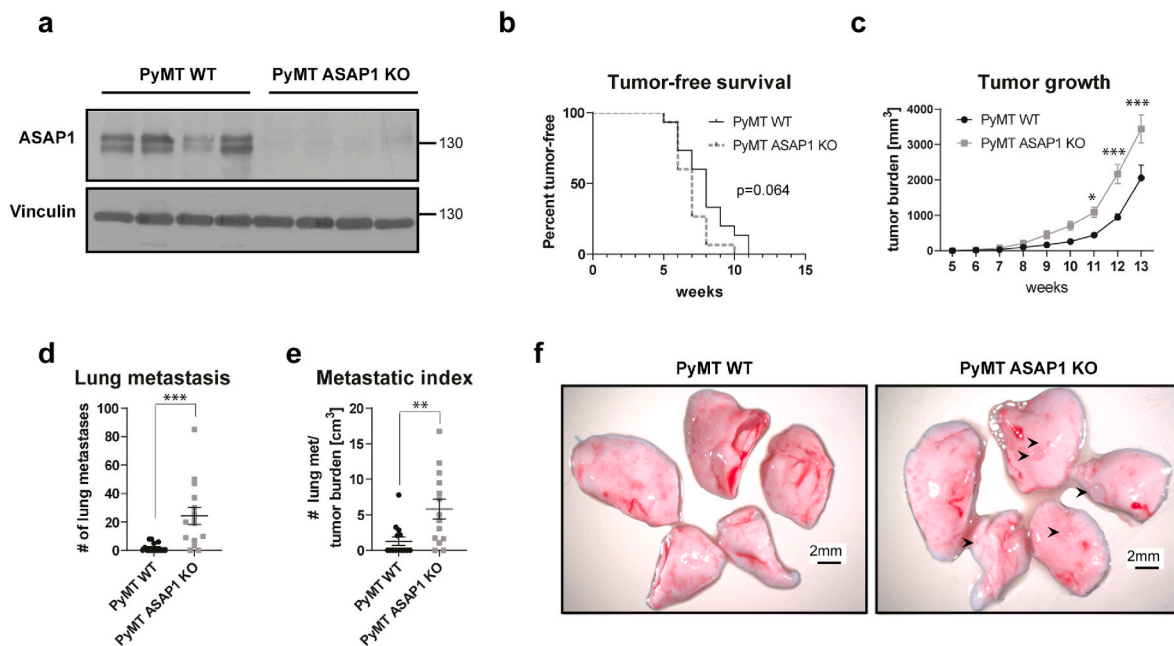


**Fig. 1. Loss of ASAP1 in PyMT mice accelerates tumor development and promotes tumor growth and metastasis.** (a) ASAP1 expression in WT and ASAP1-deficient MMTV-PyMT tumors analyzed by Western blot. Vinculin was used as loading control. (b) Kaplan-Meier plots of tumor free-survival of PyMT WT and PyMT ASAP1 KO female mice (PyMT WT n = 15, PyMT ASAP1 KO n = 15). Mice were considered to be tumor-free until tumor burdens stayed constantly above 20 mm<sup>3</sup>. Significance was calculated using the log-rank test. (c) Growth of PyMT WT and PyMT ASAP1 KO tumors. Data represent the mean  $\pm$  SEM (PyMT WT n = 15, PyMT ASAP1 KO n = 15). Significance was calculated using two-way ANOVA with multiple comparisons tests. \* $P < 0.05$ , \*\*\* $P < 0.001$ . (d, e) Quantification of macroscopic lung metastases (d) and metastatic index (e) in PyMT WT and PyMT ASAP1 KO mice at the age of 13 weeks. Data represent the mean  $\pm$  SEM (PyMT WT n = 15, PyMT ASAP1 KO n = 15). Significance was calculated using Student's t-test. \*\* $P < 0.01$ , \*\*\* $P < 0.001$ . (f) Representative pictures of lungs of PyMT WT and PyMT ASAP1 KO mice. Scale bar, 2 mm. .

that deletion of ASAP1 in MMTV-PyMT mice either accelerates tumor initiation or promotes tumor growth, and increases lung metastasis.

### 3.2. Loss of ASAP1 does not significantly alter tumor cell proliferation, apoptosis, angiogenesis or macrophage infiltration

The finding that deletion of ASAP1 promoted tumor growth and metastasis in MMTV-PyMT mice was unexpected as we and others have shown that ASAP1 is often up-regulated in various types of cancer, and can promote metastasis when overexpressed. Therefore, we set out to analyze the underlying mechanisms through which loss of ASAP1 can promote tumor progression and metastasis in the MMTV-PyMT mouse model of luminal breast cancer. To this end, we first investigated whether the difference in tumor growth between WT and ASAP1-deficient PyMT tumors resulted from different proliferation rates. We analyzed the percentage of Ki67+ cells in tumors from PyMT WT and PyMT ASAP1 KO mice at early (10 weeks) and late carcinoma (13 weeks) stages, but no difference was observed (Fig. 2a and b). Next, we assessed whether PyMT ASAP1 KO tumors grew faster due to a reduced apoptosis rate. There was a slight but non-significant reduction in the number of TUNEL+ cells in PyMT ASAP1 KO tumors (Fig. 2a and c). While PyMT tumors resemble a luminal subtype and most tumor cells express the luminal cell markers CK8/CK18 [27], a small minority of

tumor cells express basal markers such as cytokeratins 5 or 14. However, we could not detect significant differences in the fraction of CK14+ cells, suggesting that loss of ASAP1 did not switch the origin of tumor cells from luminal to basal (Fig. 2a and d). Although ASAP1 has been shown to be expressed in endothelial cells and to play a role in angiogenesis and tubular formation [38], we could not detect any significant difference in tumor angiogenesis based on PECAM-1 staining (Fig. 2a and e). Finally, we analyzed whether loss of ASAP1 alters the recruitment of tumor-associated macrophages. ASAP1 has been shown to be expressed in macrophages, and may regulate their function [10,39,40]. However, loss of ASAP1 in PyMT mice did not significantly alter the recruitment of F4/80+ tumor macrophages (Fig. 2a and f). Together, these results suggest that loss of ASAP1 does not alter tumor cell proliferation or stromal tumor components such as tumor-associated macrophages and blood vessels.

### 3.3. ASAP1 deficiency accelerates tumor initiation

As the above analysis did not reveal any differences in advanced tumors taken from WT and ASAP1-deficient PyMT mice, we performed whole mount stainings of mammary glands taken from WT and ASAP1-deficient PyMT mice at six weeks of age. Mammary glands from PyMT ASAP1 KO mice displayed an increased hyperplastic area compared to

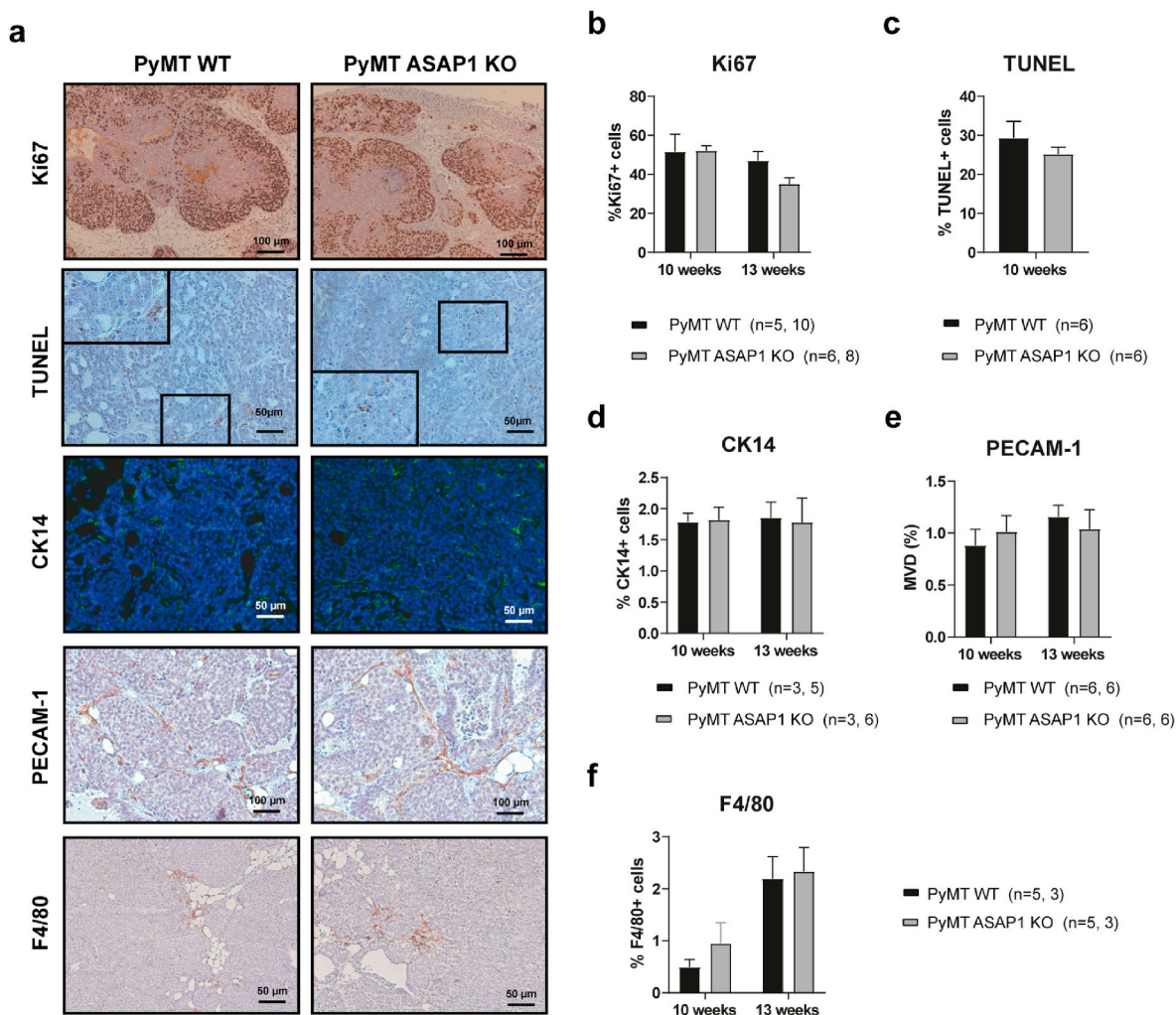


**Fig. 2. WT and ASAP1-deficient tumors exhibit similar phenotypes.** (a) Immunostaining of tumor sections of PyMT WT and PyMT ASAP1 KO tumors. Representative pictures of Ki67, TUNEL, CK14, PECAM-1 and F4/80 staining in PyMT WT and PyMT ASAP1 KO tumors. (b-f) Quantification of Ki67 staining (b), TUNEL staining (c), CK14 staining (d), microvascular density (MVD) based on PECAM-1 staining (e) and F4/80 staining (f) in PyMT WT and PyMT ASAP1 KO tumors at the age of 10 weeks and 13 weeks (end point), as indicated. Data represent mean ± SEM.

mammary glands from PyMT WT mice, suggesting that either tumor initiation or outgrowth may start earlier as a consequence of loss of ASAP1 (Fig. 3a and b). Histological analysis revealed a slight but non-significant trend towards an increased percentage of Ki67+ cells in PyMT ASAP1 KO hyperplastic lesions (Fig. 3c and d).

To assess whether loss of ASAP1 causes premature mammary gland development that might foster an earlier onset of tumor development, we compared mammary glands from 6-week old WT and ASAP1 KO female mice. ASAP1 deficiency did not significantly increase ductal invasion (Supplementary Figs. 1a and b) or affect branching density (Supplementary Figs. 1a and c). These data suggest that loss of ASAP1 does not promote premature mammary gland development.

### 3.4. Loss of ASAP1 in stromal cells does not accelerate tumorigenesis or metastasis

In PyMT ASAP1 KO mice, ASAP1 is deleted in both tumor and stromal cells. Tumor initiation, growth and metastasis are supported by both tumor cell intrinsic factors (e.g. genetic alterations) and extrinsic factors (e.g. alterations in the tumor stroma). In order to investigate the relative contribution of ASAP1 loss within the tumor cell and the stromal compartments to the observed increase in PyMT tumor growth and metastasis, we first assessed which cells express ASAP1 in PyMT WT tumors. We detected ASAP1 in tumor cells as well as in stromal cells such as fibroblasts and histiocytes, indicating that ASAP1 may play a role in stromal cells that conceivably could affect tumor growth and metastasis (Fig. 4a).

Previously we have reported that ASAP1 regulates the differentiation of mesenchymal cells [25]. Mesenchymal cells such as activated fibroblasts can play an important role during tumor growth [41]. For example, cancer-associated fibroblasts (CAFs), which are characterized

by expression of  $\alpha$ SMA, PDGFR $\alpha$  and FAP, support remodeling of the tumor stroma, inflammation and angiogenesis, and foster cancer cell proliferation, survival, invasion and metastasis. To investigate whether loss of ASAP1 affects activation of fibroblasts, we analyzed primary mouse embryonic fibroblasts (MEFs) for the expression of the CAF marker  $\alpha$ SMA and tenascin, and found that they were increased in ASAP1 KO MEFs compared to ASAP1 WT MEFs (Supplementary Fig. 2).

Therefore, we tested whether loss of ASAP1 in fibroblasts can support tumor growth. To this end, we established a tumor cell line from a WT PyMT tumor, and passaged the cells once *in vivo* to increase the tumor take rate. The PyMT cells were then co-injected orthotopically together with either WT MEFs or ASAP1 KO MEFs into WT recipient mice (Fig. 4b). However, tumor growth was not enhanced but rather delayed by co-injection of tumor cells together with ASAP1 KO MEFs compared to WT MEFs. Furthermore, lung metastasis was also not significantly increased, indicating that loss of ASAP1 in tumor-associated fibroblasts was not responsible for the enhanced tumor development observed in PyMT ASAP1 KO mice (Fig. 4c-d).

To assess if ASAP1 expression in other stromal cells might affect tumor progression and dissemination, we tested whether systemic loss of ASAP1 in host mice affected primary tumor growth or metastasis of WT PyMT tumor cells. To this end WT PyMT tumor cells were injected orthotopically into WT or ASAP1 KO recipient mice (Fig. 4e). Systemic loss of ASAP1 in the recipient mice resulted in a delayed, rather than accelerated, tumor development (Fig. 4f-g), indicating that loss of ASAP1 in stromal cells does not promote tumor growth or metastasis.

### 3.5. Loss of ASAP1 in tumor cells causes increased PyMT tumor growth and metastasis

Next, we investigated whether loss of ASAP1 in tumor cells

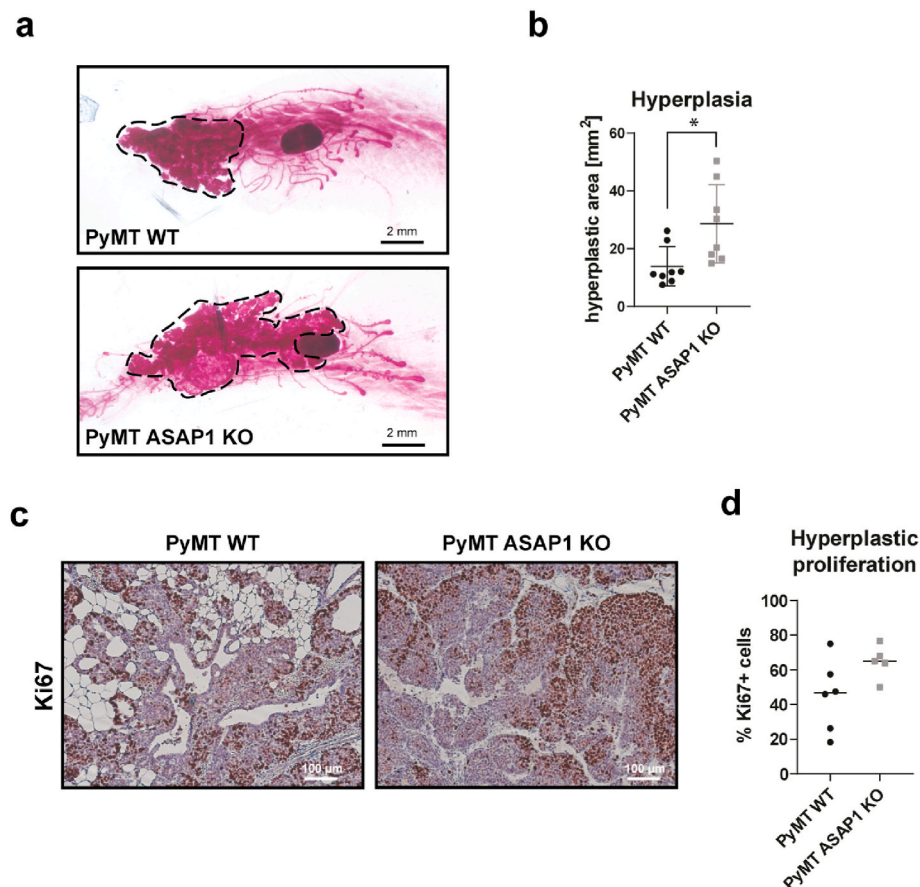


**Fig. 3. Loss of ASAP1 accelerates tumor initiation.** (a) Whole mount mammary glands were stained with carmine alum. Representative pictures of mammary hyperplasia in 6 weeks old PyMT WT and PyMT ASAP1 KO mice. Dotted lines indicate hyperplastic areas. (b) Quantification of hyperplastic area in mammary glands (n = 8 per genotype). Data represent mean  $\pm$  SEM. Significance was calculated using Student's t-test. \* $P < 0.05$ . (c, d) Representative images (c) and quantification (d) of Ki67 staining in PyMT WT (n = 6) and PyMT ASAP1 KO (n = 5) hyperplasia at the age of 6 weeks. Data represent mean  $\pm$  SEM.

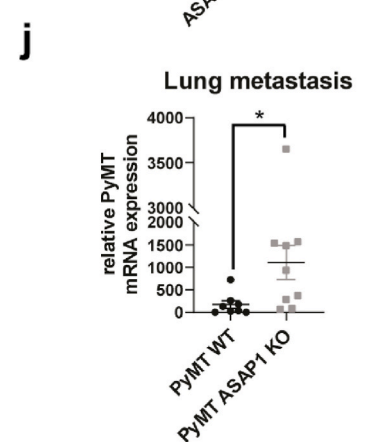
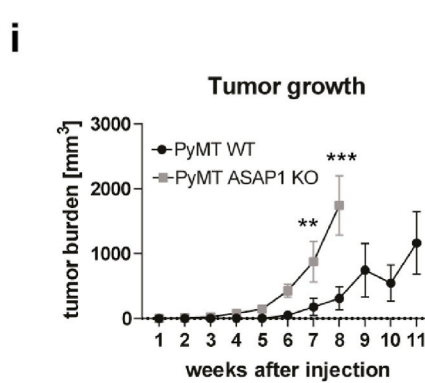
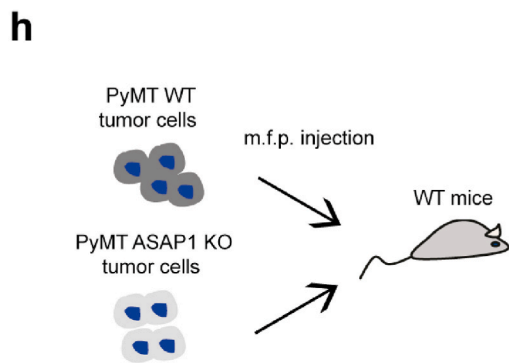
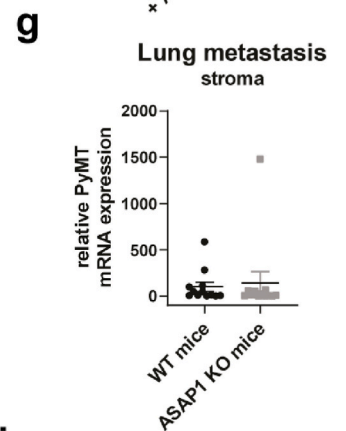
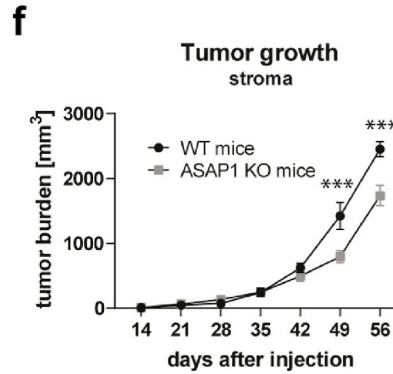
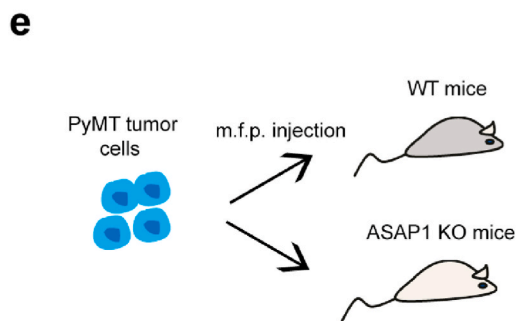
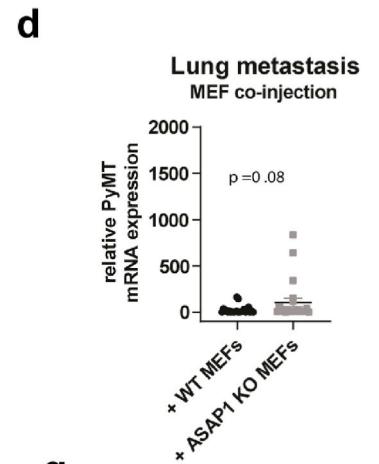
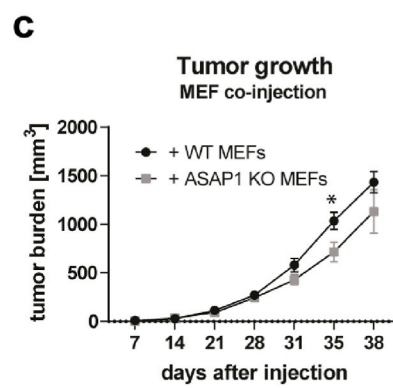
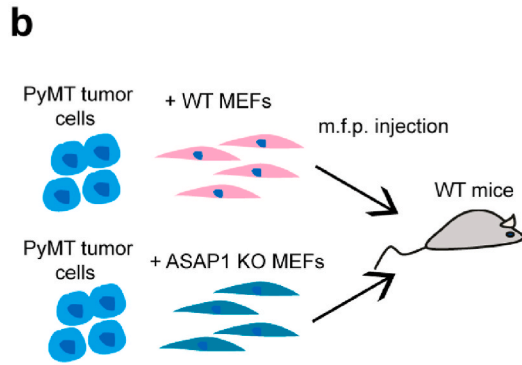
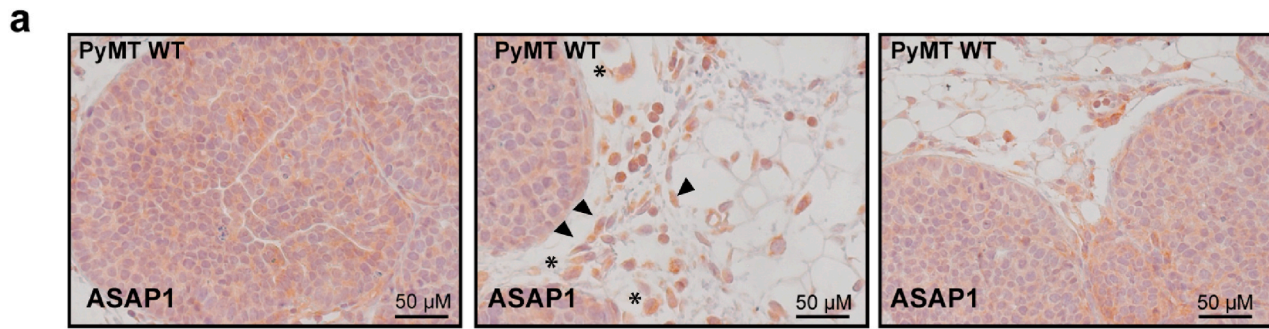


**Fig. 4. Loss of ASAP1 in PyMT tumor cells but not in stromal cells accelerates tumorigenesis and promotes metastasis.** (a) Sections of PyMT WT tumors were stained for ASAP1. Besides tumor cells, ASAP1 is expressed by fibroblasts (arrowheads) and histiocytes (asterisks). (b) Scheme showing the experimental procedure. PyMT WT tumor cells were co-injected with WT MEFs or ASAP1 KO MEFs in the mammary fat pads of wild-type mice and tumor growth (c) and lung metastasis (d) were quantified (n = 8 mice per genotype). Lung metastasis was detected through qPCR analysis of PyMT expression in the lungs when mice had to be sacrificed due to tumor diameter reaching the maximum permitted size of 2 cm. Three lung lobes per mouse were analyzed. (e) Scheme showing the experimental procedure. PyMT WT tumor cells were transplanted in the mammary fat pads (m.f.p.) of WT or ASAP1 KO mice and tumor growth (f) and lung metastasis (g) were quantified (n = 4 mice per genotype). Lung metastasis was detected through qPCR analysis of PyMT expression in the lungs. Three lung lobes per mouse were analyzed. (h) Scheme showing the experimental procedure. PyMT WT or PyMT ASAP1 KO tumor cells were injected into WT recipient mice. (i) Tumor growth curves of PyMT WT and PyMT ASAP1 KO tumor cells (n = 3 mice per genotype). (j) Metastatic dissemination of PyMT WT and PyMT ASAP1 KO tumor cells detected through qPCR analysis of PyMT expression in the lungs. Three lung lobes per mouse were analyzed. Graphs show the mean ± SEM. Significance was calculated using Student's t-test for comparison between two groups and two-way ANOVA multiple comparisons tests for the analysis of tumor growth at different time points. \* $P < 0.05$ , \*\* $P < 0.01$ , \*\*\* $P < 0.001$ .

themselves is responsible for the increased tumor growth and metastasis observed in ASAP1-deficient PyMT mice. To this end, we established cell lines from PyMT WT and PyMT ASAP1 KO tumors from littermates. The PyMT WT and PyMT ASAP1 KO tumor cells were then injected into the mammary fat pads of WT recipient mice (Fig. 4h) and tumor growth was measured. ASAP1-deficient PyMT tumor cells established measurable tumors significantly earlier than PyMT WT tumor cells (Fig. 4i). The ASAP1 deficient PyMT tumor cells also showed increased lung metastasis (Fig. 4j), reproducing the findings observed in the PyMT ASAP1 KO mouse model. These results indicate that loss of ASAP1 within tumor cells promotes PyMT tumor initiation and metastasis.

### 3.6. ASAP1 loss increases PyMT tumor cell invasion and AKT signaling

Next, we compared the functional properties of PyMT WT and PyMT ASAP1 KO tumor cells. Consistent with the findings in tumor tissue, there was no difference in the proliferation rate between PyMT WT and PyMT ASAP1 KO tumor cells in culture (Fig. 5a). However, the PyMT ASAP1 KO tumor cells displayed an increased capacity to adhere to fibronectin (Fig. 5b). Immunofluorescence analysis demonstrated that PyMT ASAP1 KO cells had a markedly higher number and total area of focal adhesions (Fig. 5c–e), as well as a larger area (Fig. 5f) and a more elongated shape, as evidenced by a higher cellular aspect ratio (ratio of length to width, Fig. 5g). Furthermore, PyMT ASAP1 KO tumor cells exhibited an enhanced invasive capacity compared to PyMT WT cells (Fig. 5h and i). Re-expression of ASAP1 in PyMT ASAP1 KO tumor cells reduced the invasive capacity of ASAP1-deficient tumor cells, indicating that loss of ASAP1 was indeed responsible for the increased invasiveness (Fig. 5h and i).

Adhesion to fibronectin and invasion are regulated by integrin and receptor tyrosine kinase-dependent pathways that involve activation of FAK and Src family kinases (SFKs), and stimulation of Ras/ERK and PI3K/AKT signaling [42]. To elucidate whether these signaling pathways are affected by inactivation of ASAP1, we performed Western blot analysis with lysates of PyMT WT and PyMT ASAP1 KO tumor cells. We found that whereas FAK signaling was unchanged, and phosphorylation of Src and ERK was only slightly induced in PyMT ASAP1 KO tumor cells compared to WT controls, phosphorylation of AKT was strongly enhanced in the PyMT ASAP1 KO tumor cells (Fig. 5j). In rescue experiments, re-expression of ASAP1 in PyMT ASAP1 KO tumor cells reduced phosphorylation of AKT (Fig. 5k), consistent with an ASAP1-dependent regulation of AKT phosphorylation.

To determine whether enhanced AKT activation contributes to the increased invasive capacity of PyMT ASAP1 KO tumor cells, we performed invasion assays with PyMT WT and PyMT ASAP1 KO tumor cells treated with an AKT1/2 inhibitor. Inhibition of AKT1/2 decreased the invasive capacity to a similar extent as re-expression of ASAP1 in the PyMT ASAP1 KO tumor cells (Fig. 5l, m).

### 3.7. Low expression of ASAP1 in ER+ luminal breast cancer correlates with poor prognosis

To investigate whether our findings obtained in the MMTV-PyMT

model of luminal breast cancer are reflected in human breast cancer patients, we performed *in silico* analysis of the TCGA breast cancer cohort [34]. ASAP1 is frequently amplified in certain types of cancer [17,18,23]. Analysis of data from the TCGA breast cancer cohort revealed that ASAP1 amplification is most frequent in basal (28%) and HER2+ tumors (18%) whereas only 9% of luminal breast cancers harbor an ASAP1 amplification (Fig. 6a). Consistently, ASAP1 is more highly expressed in ER-negative breast tumors compared to ER-positive tumors (Fig. 6b and c). In addition, the level of ASAP1 mRNA expression correlates with its amplification state in luminal breast cancers, so that samples deleted or diploid for ASAP1 had lower levels than samples with gain or high copy number amplification of ASAP1 (Fig. 6d). Furthermore, AKT1/2/3 proteins phosphorylated at threonine 308 (corresponding to active AKT) were significantly increased in luminal breast cancer samples with lower ASAP1 levels (ASAP1 deleted/diploid), compared to those with ASAP1 gain and amplification (Fig. 6e). These data suggest a link between lower ASAP1 levels and increased AKT activity in human luminal breast cancers, in agreement with the results we obtained in the MMTV-PyMT model. Consistently, analysis of ER+ breast cancer patients revealed that low ASAP1 mRNA expression in this subtype correlates with poor overall survival (Fig. 6f), further corroborating our findings in the MMTV-PyMT luminal breast cancer mouse model.

## 4. Discussion

Tumor initiation and progression is driven both by intrinsic properties of tumor cells and by interactions between tumor cells and different components of the stromal environment [43]. In this study, we used the autochthonous MMTV-PyMT mouse model of luminal breast cancer to examine the impact of ASAP1 deletion in tumor cells and stromal cells on tumor initiation, growth and metastasis. Our work revealed that loss of ASAP1 in luminal breast cancer cells resulted in accelerated tumor development and increased lung metastasis.

Previous work by us and others has correlated higher levels of ASAP1 in different types of tumors with increased epithelial-mesenchymal transition and invasive capacities of tumor or endothelial cells in pathological conditions, ultimately linked to increased metastasis [15,38,44,45]. In breast cancer, ASAP1 is often amplified and has been associated with poor relapse-free survival [22,23]. Since these findings contrast with the accelerated tumor growth and increased metastatic propensity observed following ASAP1 ablation in the MMTV-PyMT model, we sought to explore the reasons behind these differences. As our initial experiments were made in mice in which ASAP1 was simultaneously ablated in both the tumor and the stromal tissue, we reasoned that potential anti-tumorigenic functions of ASAP1 in stromal tissues may have mediated the more aggressive tumor development in animals with ASAP1 loss. However, while we detected higher levels of CAF markers in ASAP1-deficient fibroblasts, we observed no increase in metastasis when PyMT WT tumor cells were transplanted together with ASAP1-deficient fibroblasts compared to WT fibroblasts. Furthermore, when ASAP1 WT tumor cells were transplanted into the WT or ASAP1 KO background, we again found no increase in metastasis in the ASAP1 KO background. By

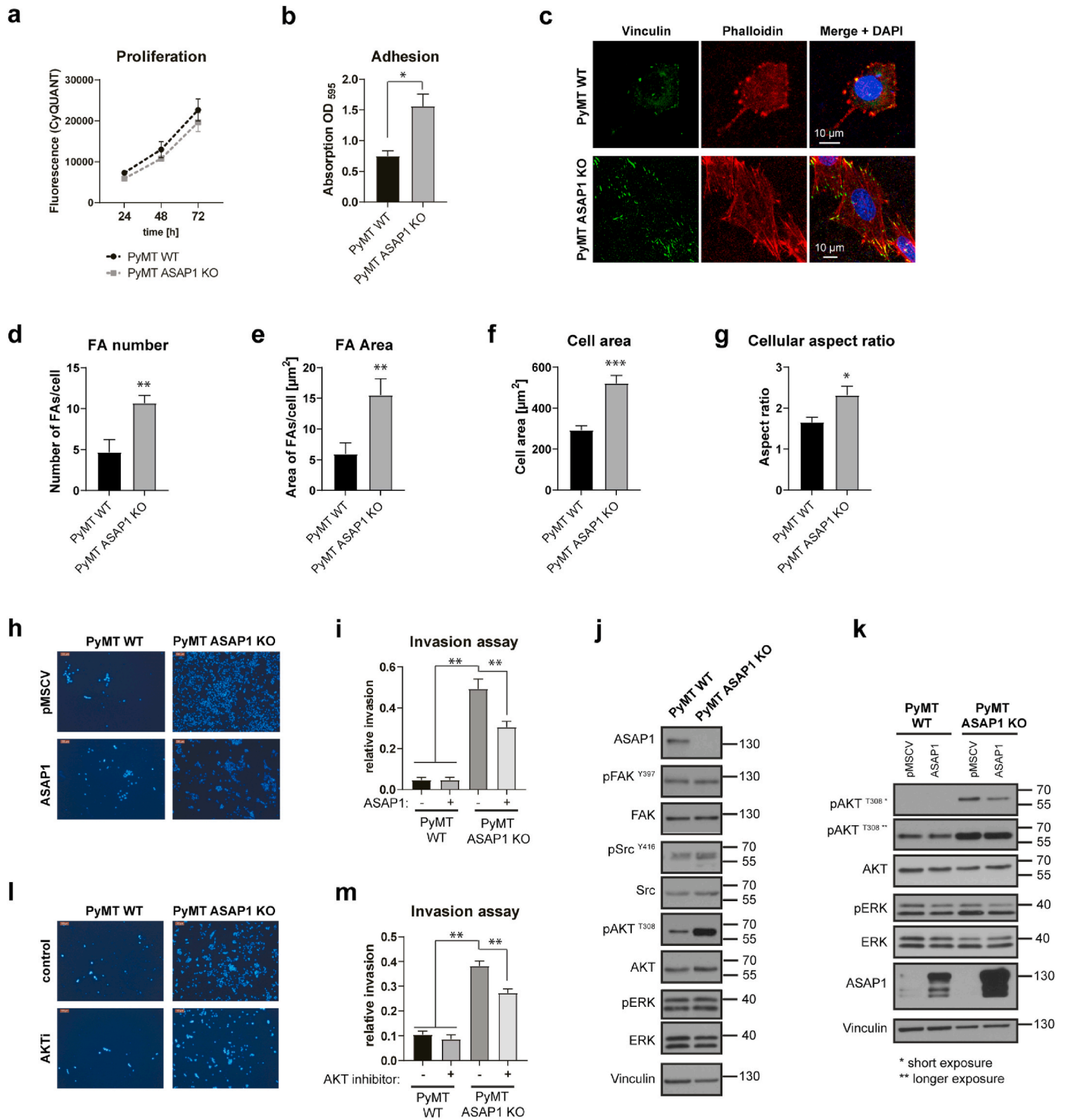


**Fig. 5. PyMT ASAP1 KO tumor cells display increased adhesive and invasive capacities.** (a) Proliferation was determined using a CyQuant assay. (b) Adhesion assay of PyMT WT and PyMT ASAP1 KO tumor cells showing increased adhesion to fibronectin upon loss of ASAP1. (c-g) Analysis of focal adhesions (FAs) and cell morphology of PyMT WT and PyMT ASAP1 KO tumor cells. Representative images of PyMT WT and PyMT ASAP1 KO tumor cells stained with vinculin and phalloidin are shown in (c), together with quantifications of FA number per cell (d), total area of FAs per cell (e), cell area (f) and cellular aspect ratio (major/minor axis, g). For d-g,  $n = 15$ . (h, i) Invasion assay of PyMT WT and PyMT ASAP1 KO tumor cells. Re-expression of ASAP1 in PyMT ASAP1 KO tumor cells by retroviral transduction decreases their invasive capacity. Representative images of transwell inserts after removing cells from the top (h) and quantification (i,  $n = 3$ ) are shown. (j) Western blot analysis of PyMT WT and PyMT ASAP1 KO tumor cell lysates analyzing different signaling pathways. (k) Western blot of lysates of PyMT WT and PyMT ASAP1 KO tumor cell re-expressing ASAP1 analyzing components of the ERK and AKT signaling pathways. (l, m) PyMT WT and PyMT ASAP1 KO tumor cells were seeded into Boyden chambers, and treated with AKT1/2 inhibitor or DMSO as control. Representative images of transwell inserts after removing cells from the top (l) and quantification (m,  $n = 3$ ) are shown. Graphs show the mean  $\pm$  SEM. Significance was calculated using Student's t-test for comparisons between two groups (b) or one-way ANOVA for comparisons between multiple groups (i and m). \* $P < 0.05$ , \*\* $P < 0.01$ , \*\*\* $P < 0.001$ .

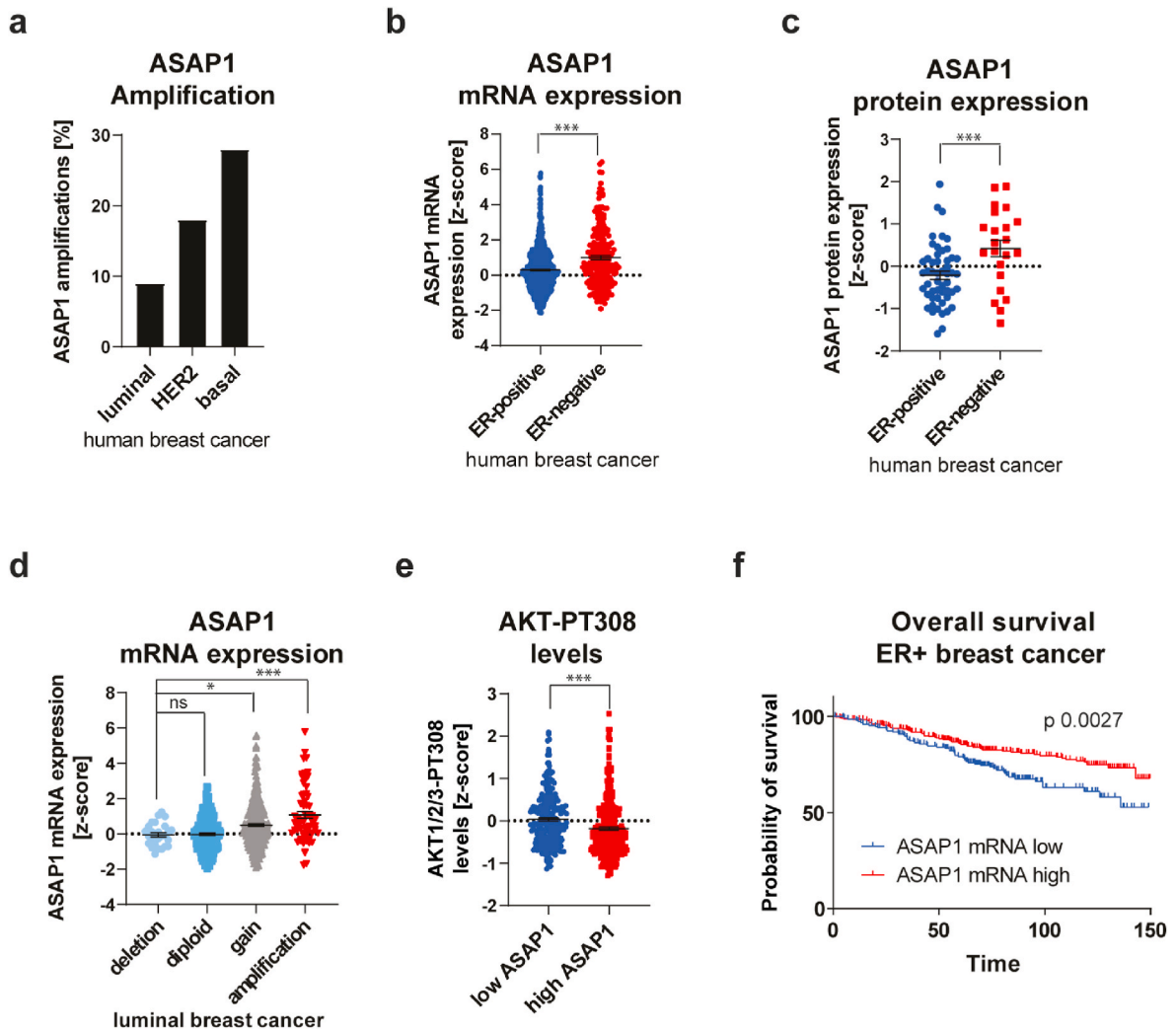


**Fig. 6. Low ASAP1 expression correlates with increased AKT activation and poor survival of human luminal/ER+ breast cancer patients.** (a) ASAP1 is less frequently amplified in luminal than in HER2+ and basal breast tumors from the TCGA breast cancer cohort. ASAP1 mRNA (b) and ASAP1 protein (c) are expressed at lower levels in ER+ than in ER-human breast tumors from the TCGA breast cancer cohort. (d) ASAP1 gain or amplification correlates with increased mRNA expression compared to tumors that are deleted or diploid for ASAP1 in human luminal breast cancer from the TCGA cohort. (e) The levels of phosphoAKT<sup>T308</sup> (AKT-PT308) are significantly higher in tumors with low ASAP1 levels compared to tumors harboring an ASAP1 gain or amplification in the TCGA breast cancer cohort. (f) Low expression of ASAP1 mRNA correlates with poor overall survival in ER+ breast cancer. Analysis was performed using KM plotter. Graphs show the mean  $\pm$  SEM. \* $P < 0.05$ , \*\* $P < 0.001$ .

contrast PyMT ASAP1 KO tumor cells transplanted into WT animals showed accelerated tumor growth and metastasis compared to PyMT WT cells. Interestingly, deletion of ASAP1 in fibroblasts or in the entire stromal compartment led to a decrease rather than an increase of primary tumor growth, indicating that ASAP1 can have disparate functions in tumor and stromal cells. It is therefore conceivable that in some cases in which ASAP1 expression in tumors has been correlated with more aggressive growth, this might be due to the function of ASAP1 in the stroma rather than the tumor cell compartment. Together these findings demonstrate that the pro-tumorigenic effects of ASAP1 loss in the MMTV-PyMT model of breast cancer are elicited by direct tumor cell-intrinsic changes, rather than by a function of ASAP1 in the tumor stroma.

A conceivable explanation for the inhibitory effect of ASAP1 on tumor progression in MMTV-PyMT mice is that the impact of ASAP1 expression on tumor formation and metastasis is context dependent, and varies according to the (sub)type of cancer concerned. Although previous studies have reported a tumor promoting role for ASAP1 in breast cancer, none of these studies have specifically assessed its function in ER+, luminal breast cancer, for which the MMTV-PyMT model is

representative. Importantly, we found that ASAP1 levels were significantly lower in human ER+/luminal breast tumors compared to other subtypes of breast cancer, and that lower expression of ASAP1 within the luminal breast cancer subtype was associated with worse overall survival, consistent with our findings in the PyMT mouse model. These results indicate that the function of ASAP1 is tumor subtype dependent, and that in ER+/luminal breast cancer it plays a tumor suppressive role. Interestingly, ASAP1 may also play a tumor suppressive role in other cancer types, as suggested by the reported loss of ASAP1 expression in more undifferentiated, metastatic unresectable hepatoblastoma [46].

To elucidate how a tumor cell-intrinsic lack of ASAP1 accelerates tumor growth and metastasis, we performed immunohistochemical and biochemical analyses. Intriguingly, we could not detect any differences in tumor proliferation, apoptosis, differentiation, angiogenesis or immune cell infiltration when tumors from PyMT WT and ASAP1-deficient PyMT mice were compared at both early and late stages of tumor growth. Instead, we found increased hyperplastic areas in mammary glands upon loss of ASAP1, suggesting that the accelerated mammary tumor development in PyMT ASAP1 KO animals can be attributed to earlier tumor initiation. Tumorigenesis involves the stepwise

accumulation of mutations, which is more likely to occur in long-lived tissue stem cells or transit-amplifying stem cells that dedifferentiate into a stem cell-like state. These mutant stem-like cells can give rise to tumor-initiating cells that sustain tumor growth and progression [47]. ASAP1 has been shown to negatively regulate the *in vivo* repopulating activity of mammary stem/progenitor cells (MaSCs), and knock-down of ASAP1 in MaSCs increases the number of colony forming units [48]. Thus, loss of ASAP1 in the PyMT model may increase the number of tumor-initiating cells and thereby promote increased tumor formation, growth and metastasis. In addition, the increased invasive potential of ASAP1-deficient PyMT cells that we observed would also serve to foster metastasis formation.

Mechanistically, we show that loss of ASAP1 in the PyMT model induces profound activation of AKT. Consistently, we found that increased activation of AKT was associated with human luminal breast tumors that did not harbor ASAP1 gain or amplification and had lower ASAP1 levels. A previous report has shown that depletion of inositol-polyphosphate 5-phosphatase (PIPP) in MMTV-PyMT mice results in AKT1 activation and increased tumor initiation and growth [49]. In our present study, metastasis was increased following ASAP1 deletion, which was linked to an AKT1-mediated potentiation of tumor cell invasion. In addition, we observed that the ASAP1 KO PyMT tumor cells were markedly more adherent than WT cells. This was accompanied by an increase in the number of focal adhesions and cell area, in line with previous findings that showed an important role of ASAP1 in focal adhesion organization and cell spreading [7,16,50]. Moreover, the observed activation of AKT in PyMT ASAP1 KO tumor cells is consistent with the known role of AKT in regulating focal adhesion dynamics to promote cell spreading and migration [51,52]. Interestingly, several studies have indicated that the different AKT isoforms play distinct roles in tumor progression [53]. While activated AKT1 accelerates tumor initiation, activated AKT2 fosters lung metastasis [54,55]. In our experiments, we used an antibody that recognizes the active state of all AKT isoforms. Therefore, it is possible that both AKT1 and AKT2 are activated in our model, simultaneously promoting tumor formation, invasion and metastasis. The mechanism through which loss of ASAP1 promotes activation of AKT in PyMT tumor cells is currently unclear. Previously we found that loss of ASAP1 in fibroblasts decreased AKT signaling due to diminished FAK/Src signaling [25]. In contrast to the primary fibroblasts, FAK was not deregulated in PyMT ASAP1 KO tumor cells, whereas AKT signaling was enhanced, further highlighting the differential role of ASAP1 in the tumor cell and stromal compartments. Taken together, our data indicate that ASAP1 can play distinct roles in different types of cancer, and that in ER+ luminal breast cancer it acts in a tumor suppressive manner. Low ASAP1 expression may increase the population of progenitor cells, resulting in increased tumor initiation. In addition, loss or lower levels of ASAP1 expression positively regulate AKT activity in ER+ luminal cancer, which can promote tumor formation, invasion and metastasis.

## Declarations

### Author contributions

CS, JPS: Conceptualization; CS, BKG: Data curation; CS, ZHF, NM, MT, BKG: Formal analysis; CS, JPS: Funding acquisition; CS, AG, SR, SS, SH, WT, ZHF, NM, AS, MR, AD, MT, BKG, JPS: Investigation; CS, AG, SR, SS, SH, ZHF, NM, AS, BKG: Methodology; WT, JPS: Project administration; MT, BKG, JPS: Supervision; CS, BKG, JPS: Writing - original draft; CS, BKG, JPS: Writing - review & editing.

## Funding

JPS is holder of the “Franz-Volhard-Stiftungsprofessur für Mikrovaskuläre Biologie und Pathobiologie”, which was funded by the Klinikum Mannheim gGmbH during part of this work. CS was funded by

the MEAMEDMA program of the Medical Faculty Mannheim. SS was funded by a scholarship from the Deutscher Akademischer Austausch Dienst (DAAD).

## Declaration of interests

The authors declare that they have no known competing financial interests or personal relationships that could have appeared to influence the work reported in this paper.

## Declaration of competing interest

The authors declare no competing interests.

## Acknowledgements

The authors gratefully acknowledge the assistance and expertise of Manuela Sauer and Selma Huber with animal husbandry.

## References

- [1] B. Barnes, K. Kraywinkel, E. Nowossadeck, I. Schonfeld, A. Starker, A. Wienecke, U. Wolf, Bericht Zum Krebsgeschehen in Deutschland 2016, Robert Koch-Institut, 2016.
- [2] C.M. Perou, T. Sorlie, M.B. Eisen, M. van de Rijn, S.S. Jeffrey, C.A. Rees, J. R. Pollack, D.T. Ross, H. Johnsen, L.A. Akslen, O. Fluge, A. Pergamenschikov, C. Williams, S.X. Zhu, P.E. Lonning, A.L. Borresen-Dale, P.O. Brown, D. Botstein, Molecular portraits of human breast tumours, *Nature* 406 (2000) 747–752.
- [3] T. Sorlie, C.M. Perou, R. Tibshirani, T. Aas, S. Geisler, H. Johnsen, T. Hastie, M. B. Eisen, M. van de Rijn, S.S. Jeffrey, T. Thorsen, H. Quist, J.C. Matise, P.O. Brown, D. Botstein, P.E. Lonning, A.L. Borresen-Dale, Gene expression patterns of breast carcinomas distinguish tumor subclasses with clinical implications, *Proc. Natl. Acad. Sci. U. S. A.* 98 (2001) 10869–10874.
- [4] A. Goldhirsch, E.P. Winer, A.S. Coates, R.D. Gelber, M. Piccart-Gebhart, B. Thurlimann, H.J. Senn, m. Panel, Personalizing the treatment of women with early breast cancer: highlights of the st gallen international expert consensus on the primary therapy of early breast cancer 2013, *Ann. Oncol.* 24 (2013) 2206–2223.
- [5] M.T. Brown, J. Andrade, H. Radhakrishna, J.G. Donaldson, J.A. Cooper, P. A. Randazzo, ASAP1, a phospholipid-dependent arf GTPase-activating protein that associates with and is phosphorylated by Src, *Mol. Cell Biol.* 18 (1998) 7038–7051.
- [6] T. Vitali, S. Giraldo-Berlinger, P.A. Randazzo, P.W. Chen, Arf GAPs: a family of proteins with disparate functions that converge on a common structure, the integrin adhesion complex, *Small GTPases* (2017) 1–9.
- [7] Y. Liu, J.C. Loijens, K.H. Martin, A.V. Karginov, J.T. Parsons, The association of ASAP1, an ADP ribosylation factor-GTPase activating protein, with focal adhesion kinase contributes to the process of focal adhesion assembly, *Mol. Biol. Cell* 13 (2002) 2147–2156.
- [8] Y. Onodera, S. Hashimoto, A. Hashimoto, M. Morishige, Y. Mazaki, A. Yamada, E. Ogawa, M. Adachi, T. Sakurai, T. Manabe, H. Wada, N. Matsuura, H. Sabe, Expression of AMAP1, an ArfGAP, provides novel targets to inhibit breast cancer invasive activities, *EMBO J.* 24 (2005) 963–973.
- [9] A. Oda, I. Wada, K. Miura, K. Okawa, T. Kadoya, T. Kato, H. Nishihara, M. Maeda, S. Tanaka, K. Nagashima, C. Nishitani, K. Matsuno, M. Ishino, L.M. Machesky, H. Fujita, P. Randazzo, CrkL directs ASAP1 to peripheral focal adhesions, *J. Biol. Chem.* 278 (2003) 6456–6460.
- [10] D.N. Tien, M. Kishihata, A. Yoshikawa, A. Hashimoto, H. Sabe, E. Nishi, K. Kamei, H. Arai, T. Kita, T. Kimura, M. Yokode, N. Ashida, AMAP1 as a negative-feedback regulator of nuclear factor-kappaB under inflammatory conditions, *Sci. Rep.* 4 (2014) 5094.
- [11] Y. Liu, G.M. Yerushalmi, P.R. Grigera, J.T. Parsons, Mislocalization or reduced expression of Arf GTPase-activating protein ASAP1 inhibits cell spreading and migration by influencing Arf1 GTPase cycling, *J. Biol. Chem.* 280 (2005) 8884–8892.
- [12] Y. Onodera, J.M. Nam, A. Hashimoto, J.C. Norman, H. Shirato, S. Hashimoto, H. Sabe, Rab5c promotes AMAP1-PRKD2 complex formation to enhance beta 1 integrin recycling in EGF-induced cancer invasion, *J. Cell Biol.* 197 (2012) 983–996.
- [13] Z. Nie, D.S. Hirsch, R. Luo, X. Jian, S. Stauffer, A. Cremesti, J. Andrade, J. Lebowitz, M. Marino, B. Ahvazi, J.E. Hinshaw, P.A. Randazzo, A BAR domain in the N terminus of the Arf GAP ASAP1 affects membrane structure and trafficking of epidermal growth factor receptor, *Curr. Biol.* 16 (2006) 130–139.

- [14] C. Furman, S.M. Short, R.R. Subramanian, B.R. Zetter, T.M. Roberts, DEF-1/ASAP1 is a GTPase-activating protein (GAP) for ARF1 that enhances cell motility through a GAP-dependent mechanism, *J. Biol. Chem.* 277 (2002) 7962–7969.
- [15] T. Muller, U. Stein, A. Poletti, L. Garzia, M. Rothley, D. Plaumann, W. Thiele, M. Bauer, A. Galasso, P. Schlag, M. Pankratz, M. Zollo, J.P. Sleeman, ASAP1 promotes tumor cell motility and invasiveness, stimulates metastasis formation in vivo, and correlates with poor survival in colorectal cancer patients, *Oncogene* 29 (2010) 2393–2403.
- [16] P.A. Randazzo, J. Andrade, K. Miura, M.T. Brown, Y.Q. Long, S. Stauffer, P. Roller, J.A. Cooper, The Arf GTPase-activating protein ASAP1 regulates the actin cytoskeleton, *Proc. Natl. Acad. Sci. U. S. A.* 97 (2000) 4011–4016.
- [17] J.P. Ehlers, L. Worley, M.D. Onken, J.W. Harbour, DDEF1 is located in an amplified region of chromosome 8q and is overexpressed in uveal melanoma, *Clin. Cancer Res.* 11 (2005) 3609–3613.
- [18] D. Lin, A. Watahiki, J. Bayani, F. Zhang, L. Liu, V. Ling, M.D. Sadar, J. English, L. Fazli, A. So, P.W. Gout, M. Gleave, J.A. Squire, Y.Z. Wang, ASAP1, a gene at 8q24, is associated with prostate cancer metastasis, *Cancer Res.* 68 (2008) 4352–4359.
- [19] T. Hou, C. Yang, C. Tong, H. Zhang, J. Xiao, J. Li, Overexpression of ASAP1 is associated with poor prognosis in epithelial ovarian cancer, *Int. J. Clin. Exp. Pathol.* 7 (2014) 280–287.
- [20] H. Sato, K.C. Hatanaka, Y. Hatanaka, H. Hatakeyama, A. Hashimoto, Y. Matsuno, S. Fukuda, H. Sabe, High level expression of AMAP1 protein correlates with poor prognosis and survival after surgery of head and neck squamous cell carcinoma patients, *Cell Commun. Signal.* 12 (2014) 17.
- [21] Q. Luo, S. Zhang, D. Zhang, F. Yuan, X. Chen, S. Yang, Expression of ASAP1 and FAK in gastric cancer and its clinicopathological significance, *Oncol. Lett.* 20 (2020) 974–980.
- [22] R. Kinoshita, J.M. Nam, Y.M. Ito, K.C. Hatanaka, A. Hashimoto, H. Handa, Y. Otsuka, S. Hashimoto, Y. Onodera, M. Hosoda, S. Onodera, S. Shimizu, S. Tanaka, H. Shirato, M. Tanino, H. Sabe, Co-overexpression of GEP100 and AMAP1 proteins correlates with rapid local recurrence after breast conservative therapy, *PLoS One* 8 (2013), e76791.
- [23] J. He, R.P. McLaughlin, L. van der Beek, S. Canisius, L. Wessels, M. Smid, J.W. M. Martens, J.A. Foekens, Y. Zhang, B. van de Water, Integrative analysis of genomic amplification-dependent expression and loss-of-function screen identifies ASAP1 as a driver gene in triple-negative breast cancer progression, *Oncogene* 39 (2020) 4118–4131.
- [24] C.T. Guy, R.D. Cardiff, W.J. Muller, Induction of mammary tumors by expression of polyomavirus middle T oncogene: a transgenic mouse model for metastatic disease, *Mol. Cell Biol.* 12 (1992) 954–961.
- [25] C. Schreiber, S. Saraswati, S. Harkins, A. Gruber, N. Cremers, W. Thiele, M. Rothley, D. Plaumann, C. Korn, O. Armant, H.G. Augustin, J.P. Sleeman, Loss of ASAP1 in mice impairs adipogenic and osteogenic differentiation of mesenchymal progenitor cells through dysregulation of FAK/Src and AKT signaling, *PLoS Genet.* 15 (2019), e1008216.
- [26] M.M. Fluck, B.S. Schaffhausen, Lessons in signaling and tumorigenesis from polyomavirus middle T antigen, *Microbiol. Mol. Biol. Rev.* 73 (2009) 542–563. Table of Contents.
- [27] J.I. Herschkowitz, K. Simin, V.J. Weigman, I. Mikielien, J. Usary, Z. Hu, K. E. Rasmussen, L.P. Jones, S. Assefnia, S. Chandrasekharan, M.G. Backlund, Y. Yin, A.I. Khramtsov, R. Bastein, J. Quackenbush, R.I. Glazer, P.H. Brown, J.E. Green, L. Kopelovich, P.A. Furth, J.P. Palazzo, O.I. Olopade, P.S. Bernard, G.A. Churchill, T. Van Dyke, C.M. Perou, Identification of conserved gene expression features between murine mammary carcinoma models and human breast tumors, *Genome Biol.* 8 (2007) R76.
- [28] E.Y. Lin, J.G. Jones, P. Li, L. Zhu, K.D. Whitney, W.J. Muller, J.W. Pollard, Progression to malignancy in the polyoma middle T oncoprotein mouse breast cancer model provides a reliable model for human diseases, *Am. J. Pathol.* 163 (2003) 2113–2126.
- [29] C.A. Schneider, W.S. Rasband, K.W. Eliceiri, NIH Image to ImageJ: 25 years of image analysis, *Nat. Methods* 9 (2012) 671–675.
- [30] J.P. Stanko, S.E. Fenton, Quantifying branching density in rat mammary gland whole-mounts using the Sholl analysis method, *JoVE* (2017).
- [31] T. Bentele, F. Amadei, E. Kimmle, M. Veschgini, P. Linke, M. Sontag-Gonzalez, J. Tennigkeit, A.D. Ho, S. Ozbek, M. Tanaka, New class of crosslinker-free nanofiber biomaterials from Hydra nematocyst proteins, *Sci. Rep.* 9 (2019) 19116.
- [32] L. Yu, J. Li, J. Hong, Y. Takashima, N. Fujimoto, M. Nakajima, A. Yamamoto, X. Dong, Y. Dang, Y. Hou, W. Yang, I. Minami, K. Okita, M. Tanaka, C. Luo, F. Tang, Y. Chen, C. Tang, H. Kotera, L. Liu, Low cell-matrix adhesion reveals two subtypes of human pluripotent stem cells, *Stem Cell Reports* 11 (2018) 142–156.
- [33] S. Morita, T. Kojima, T. Kitamura, Plat-E: an efficient and stable system for transient packaging of retroviruses, *Gene Ther.* 7 (2000) 1063–1066.
- [34] K.A. Hoadley, C. Yau, T. Hinoue, D.M. Wolf, A.J. Lazar, E. Drill, R. Shen, A. M. Taylor, A.D. Cherniack, V. Thorsson, R. Akbani, R. Bowlby, C.K. Wong, M. Wiznerowicz, F. Sanchez-Vega, A.G. Robertson, B.G. Schneider, M.S. Lawrence, H. Noushmehr, T.M. Malta, N. Cancer Genome Atlas, J.M. Stuart, C.C. Benz, P. W. Laird, Cell-of-Origin patterns dominate the molecular classification of 10,000 tumors from 33 types of cancer, *Cell* 173 (2018) 291–304 e296.
- [35] E. Cerami, J. Gao, U. Dogrusoz, B.E. Gross, S.O. Sumer, B.A. Aksoy, A. Jacobsen, C. J. Byrne, M.L. Heuer, E. Larsson, Y. Antipin, B. Reva, A.P. Goldberg, C. Sander, N. Schultz, The cBio cancer genomics portal: an open platform for exploring multidimensional cancer genomics data, *Cancer Discov.* 2 (2012) 401–404.
- [36] J. Gao, B.A. Aksoy, U. Dogrusoz, G. Dresdner, B. Gross, S.O. Sumer, Y. Sun, A. Jacobsen, R. Sinha, E. Larsson, E. Cerami, C. Sander, N. Schultz, Integrative analysis of complex cancer genomics and clinical profiles using the cBioPortal, *Sci. Signal.* 6 (2013) p11.
- [37] B. Gyorffy, A. Lanczky, A.C. Eklund, C. Denkert, J. Budczies, Q. Li, Z. Szallasi, An online survival analysis tool to rapidly assess the effect of 22,277 genes on breast cancer prognosis using microarray data of 1,809 patients, *Breast Cancer Res. Treat.* 123 (2010) 725–731.
- [38] A. Hashimoto, S. Hashimoto, R. Ando, K. Noda, E. Ogawa, H. Kotani, M. Hirose, T. Menju, M. Morishige, T. Manabe, Y. Toda, S. Ishida, H. Sabe, GEP100-Arf6-AMAP1-cortactin pathway frequently used in cancer invasion is activated by VEGFR2 to promote angiogenesis, *PLoS One* 6 (2011), e23359.
- [39] J. Curtis, Y. Luo, H.L. Zenner, D. Cuchet-Lourenco, C. Wu, K. Lo, M. Maes, B. Alisaac, E. Stebbings, J.Z. Liu, L. Kopanitsa, O. Ignatyeva, Y. Balabanova, V. Nikolayevskiy, I. Baessmann, T. Thy, C.G. Meyer, P. Nurnberg, R. D. Horstmann, F. Drobniowski, V. Plagnol, J.C. Barrett, S. Nejentsev, Susceptibility to tuberculosis is associated with variants in the ASAP1 gene encoding a regulator of dendritic cell migration, *Nat. Genet.* 47 (2015) 523–527.
- [40] A. Haque, A.S. Noman, N. Koide, E. Odkhuu, Y. Naiki, S. Hashimoto, T. Komatsu, T. Yoshida, T. Yokochi, An ADP ribosylation factor-GTPase activating protein negatively regulates the production of proinflammatory mediators in response to lipopolysaccharide, *Cancer Immunol. Immunother.* 60 (2011) 1439–1446.
- [41] R. Kalluri, The biology and function of fibroblasts in cancer, *Nat. Rev. Cancer* 16 (2016) 582–598.
- [42] H. Hamidi, J. Ivaska, Every step of the way: integrins in cancer progression and metastasis, *Nat. Rev. Cancer* 18 (2018) 533–548.
- [43] D. Hanahan, R.A. Weinberg, Hallmarks of cancer: the next generation, *Cell* 144 (2011) 646–674.
- [44] H. Li, D. Zhang, J. Yu, H. Liu, Z. Chen, H. Zhong, Y. Wan, CCL18-dependent translocation of AMAP1 is critical for epithelial to mesenchymal transition in breast cancer, *J. Cell. Physiol.* 233 (2018) 3207–3217.
- [45] T. Zhang, G. Zhao, C. Yang, P. Dong, H. Watari, L. Zeng, L.M. Pfeffer, J. Yue, Lentiviral vector mediated-ASAP1 expression promotes epithelial to mesenchymal transition in ovarian cancer cells, *Oncol. Lett.* 15 (2018) 4432–4438.
- [46] S. Ranganathan, M. Ningappa, C. Ashokkumar, B.W. Higgs, J. Min, Q. Sun, L. Schmitt, S. Subramanian, H. Hakonarson, R. Sindh, Loss of EGFR-ASAP1 signaling in metastatic and unresectable hepatoblastoma, *Sci. Rep.* 6 (2016) 38347.
- [47] C.L. Chaffer, R.A. Weinberg, How does multiplex tumorigenesis really proceed? *Cancer Discov.* 5 (2015) 22–24.
- [48] J.M. Sheridan, M.E. Ritchie, S.A. Best, K. Jiang, T.J. Beck, F. Vaillant, K. Liu, R. A. Dickens, G.K. Smyth, G.J. Lindeman, J.E. Visvader, A pooled shRNA screen for regulators of primary mammary stem and progenitor cells identifies roles for Asap1 and Prox 1, *BMC Cancer* 15 (2015) 221.
- [49] L.M. Ooms, L.C. Binge, E.M. Davies, P. Rahman, J.R. Conway, R. Gurung, D. T. Ferguson, A. Papa, C.G. Fedele, J.L. Vieusseux, R.C. Chai, F. Koentgen, J.T. Price, T. Tiganis, P. Timpson, C.A. McLean, C.A. Mitchell, The inositol polyphosphate 5-phosphatase PIPP regulates AKT1-dependent breast cancer growth and metastasis, *Cancer Cell* 28 (2015) 155–169.
- [50] P.W. Chen, X. Jian, S.M. Heissler, K. Le, R. Luo, L.M. Jenkins, A. Nagy, J. Moss, J. R. Sellers, P.A. Randazzo, The arf GTPase-activating protein, ASAP1, binds nonmuscle myosin 2A to control remodeling of the actomyosin network, *J. Biol. Chem.* 291 (2016) 7517–7526.
- [51] J.A. Broussard, W.H. Lin, D. Majumdar, B. Anderson, B. Eason, C.M. Brown, D. J. Webb, The endosomal adaptor protein APPL1 impairs the turnover of leading edge adhesions to regulate cell migration, *Mol. Biol. Cell* 23 (2012) 1486–1499.
- [52] M. Higuchi, R. Kihara, T. Okazaki, I. Aoki, S. Suetsugu, Y. Gotoh, Akt1 promotes focal adhesion disassembly and cell motility through phosphorylation of FAK in growth factor-stimulated cells, *J. Cell Sci.* 126 (2013) 745–755.
- [53] N. Hinz, M. Jucker, Distinct functions of AKT isoforms in breast cancer: a comprehensive review, *Cell Commun. Signal.* 17 (2019) 154.
- [54] I.G. Maroulakou, W. Oemler, S.P. Naber, P.N. Tschlis, Akt1 ablation inhibits, whereas Akt2 ablation accelerates, the development of mammary adenocarcinomas in mouse mammary tumor virus (MMTV)-ErbB2/neu and MMTV-polyoma middle T transgenic mice, *Cancer Res.* 67 (2007) 167–177.
- [55] R.L. Dillon, R. Marcotte, B.T. Hennessy, J.R. Woodgett, G.B. Mills, W.J. Muller, Akt1 and akt2 play distinct roles in the initiation and metastatic phases of mammary tumor progression, *Cancer Res.* 69 (2009) 5057–5064.